Supplementary Materials

Biomimetic hierarchical porous high entropy alloy for significantly enhancing overall seawater splitting

Wei Wang[a], Weiqi Wang[a], Jun Cheng[b,]*, Xing Lu[a,]*, Yunzhuo Lu[a,]*

[a] School of Materials Science and Engineering, Dalian Jiaotong University, Dalian 116028, China

[b] Northwest Institute for Nonferrous Metal Research, Shaanxi Key Laboratory of Biomedical Metal Materials, Xi'an 710016, China

Corresponding authors: chengjun_851118@126.com (J.Cheng), lu@djtu.edu.cn (X. Lu), luyz@djtu.edu.cn (Y.Z. Lu)

Experimental section

Preparation of BHP-HEA cathodes: We chose the spherical AlCoCrFeNi$_{2.1}$ powder prepared by aerosolization by Beijing Yanbang New Materials Technology Co., Ltd as the raw material. The particle size range of the powder is 15-53 μm, and the particle size distribution is uniform without the satellite particles powder (Fig. S1). In addition, the energy-dispersive spectrometry (EDS) results indicate the distribution of various elements is relatively uniform. Specimens with 10×10×1 mm and porous AlCoCrFeNi$_{2.1}$ HEA are prepared using an SLM machine equipped with a 500 W laser device (FF-M180D). During the printing process, the spot diameter is 120 μm, the scanning interval is 100 μm, the laser power is 200 W, and the scanning speed is 600 mm/s. To reduce internal stress and macroscopic porosity, the laser scanning directions of two successive layers differed by 66.7°.To obtain a nanoporous high entropy alloy, the printed precursor alloy is immersed in 0.5 M H$_2$SO$_4$ solution for selective phase dissolution. After 48 hours of free corrosion, a nanoporous structure with a dual continuous porous structure is formed on the surface of the precursor.

Microstructure characterization: The X-ray diffraction (XRD, Empyrean) with Cu Ka radiation is used to analyze the phase composition of the electrodes. The scanning electron microscopy (SEM, Zeiss Ultra 55) and transmission electron microscopy (TEM, JSM 2100F) are used to characterize the microstructure of the electrodes, and the chemical composition is analyzed using EDS equipped with them. An X-ray photoelectron spectrometer (XPS, Thermo Scientific ESCALAB 250 XI) is used to determine the types of elements and chemical states on the electrode surface.

Electrochemical measurements: The electrochemical measurements are performed in a conventional three-electrode setup(CHI 660E, Shanghai). The BHP-HEA electrode is used as the working electrode, the Pt sheet is used as the counter electrode, and the Ag/AgCl is used as the reference electrode. To ensure the accuracy of the experiment, all potentials are iR-corrected according to the equation $E_{RHE}=E_{Ag/AgCl}+0.198+0.059pH$. The polarization curve measurements are conducted at a scanning speed of 5 mV s^{-1}. In addition, EIS analysis is measured in a frequency ranging from 10 MHz to 100 kHz frequency with an AC signal amplitude of 5 mV. The overall seawater splitting

performance is measured using a two-electrode system, and stability tests are conducted under constant current density at 100 mA cm^{-2}.

Electrochemical active surface area (ECSA) measurements and calculation: The ECSA is calculated through performing the capacitive current associated with double-layer charging from the scan-rate dependence of CV. The CV of all samples is conducted with different scan rate in non-faradic potential window. The ECSA is evaluated in terms of double layer capacitance (C_{dl} in mF): ECSA = C_{dl}/C_s. The ECSA is determined assuming a C_{dl} capacitance of 40 μF cm^{-2}.

Specific activity and Turnover frequency (TOF):

The specific activity is obtained by normalizing the apparent current to ECSA. Specific activity is calculated as follows:[1] Specific activity = j×A/ECSA. Where j is the current density, A is the surface area, ECSA is the electrochemical surface area of the catalyst. The turnover frequency (TOF) are calculated using the following formula:

$$TOF_{HER} = \frac{I}{2 \times F \times n}$$

$$TOF_{OER} = \frac{I}{4 \times F \times n}$$

Where I is the current, F is the Faraday's constant (96485.3 C/mol), n is the number of active sites.

Faraday efficiency (FE): The Faraday efficiency of water splitting refers to the ratio of the gas produced during the electrolysis process to the theoretical yield. It is an important indicator for measuring the efficiency and purity of the electrolysis process. The faradaic yield is calculated from the ratio of $V_{experimental}$ to $V_{theoretical}$ during the charge transport process.[2]

$$FE_{HER} = \frac{V_{experimental}}{V_{theoretical}} = \frac{V_{experimental}}{\frac{1}{2} \times \frac{Q}{F} \times V_m}$$

$$FE_{\text{OER}} = \frac{V_{experimental}}{V_{theoretical}} = \frac{V_{experimental}}{\frac{1}{4} \times \frac{Q}{F} \times V_m}$$

where Q is the charge passed through the electrode, F is Faraday constant (96485 C/mol), V_m is the molar volume of gas (24.5 L/mol, 298 K, 101 KPa).
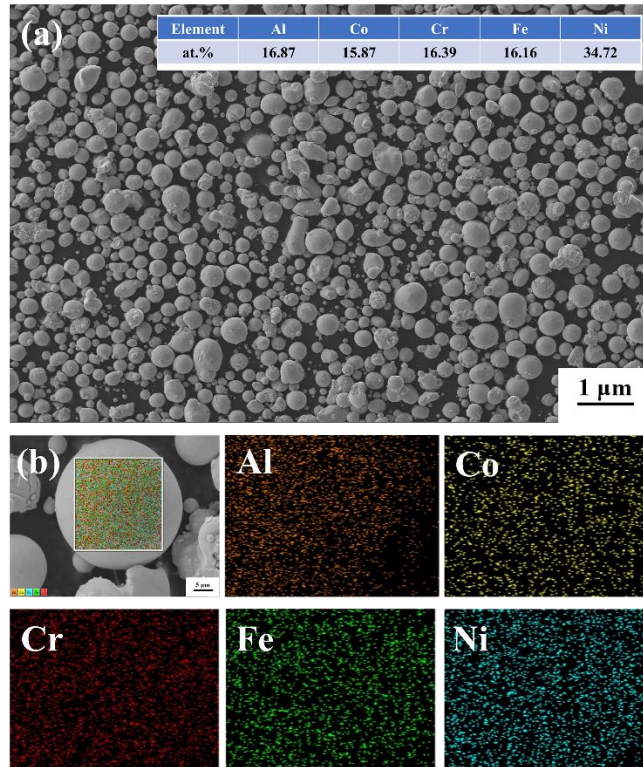
Element	Al	Co	Cr	Fe	Ni
at.%	16.87	15.87	16.39	16.16	34.72

Fig. S1 (a)SEM morphologies of AlCoCrFeNi$_{2.1}$ powders. (b) Corresponding EDS mapping.
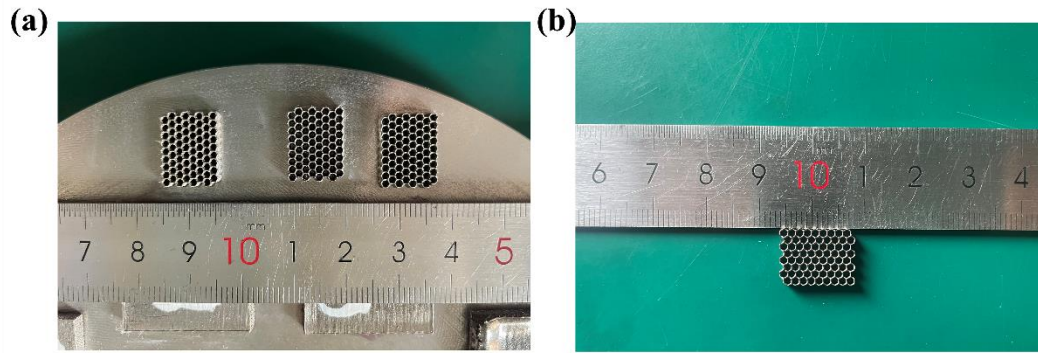
Fig. S2 (a)The microscopic morphology of porous AlCoCrFeNi$_{2.1}$ HEA. (b)The microscopic morphology of BHP-HEA
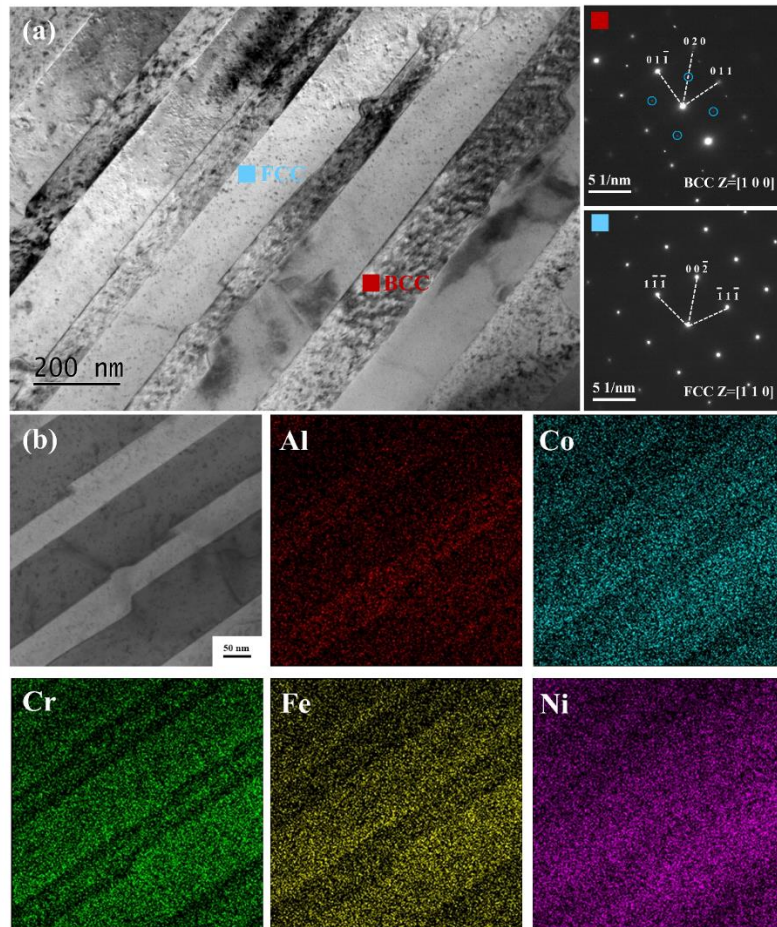
Fig. S3 TEM image and corresponding EDS elemental mappings of the AlCoCrFeNi$_{2.1}$ HEA.
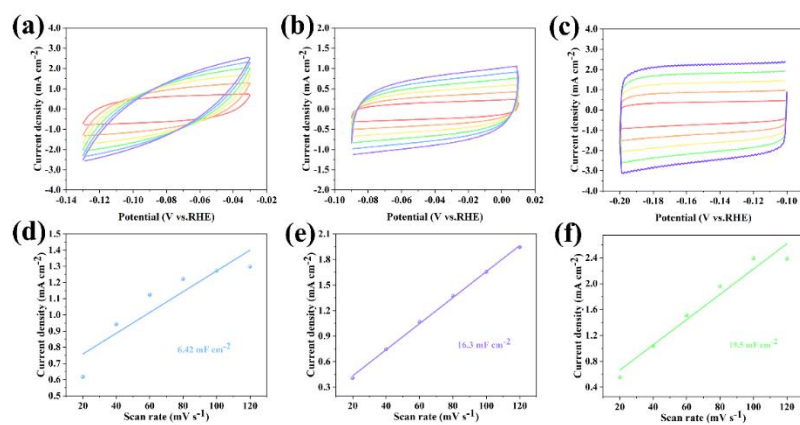
Fig. S4 (a-c) CV curves at scan rates of 20, 40, 60, 80, 100, and 120 mV s⁻¹ for Precursor alloy (a), NP-HEA (b), BHP-HEA (c). (d-f) Double layer capacitance for Precursor alloy (d), NP-HEA (e), and BHP-HEA (f).
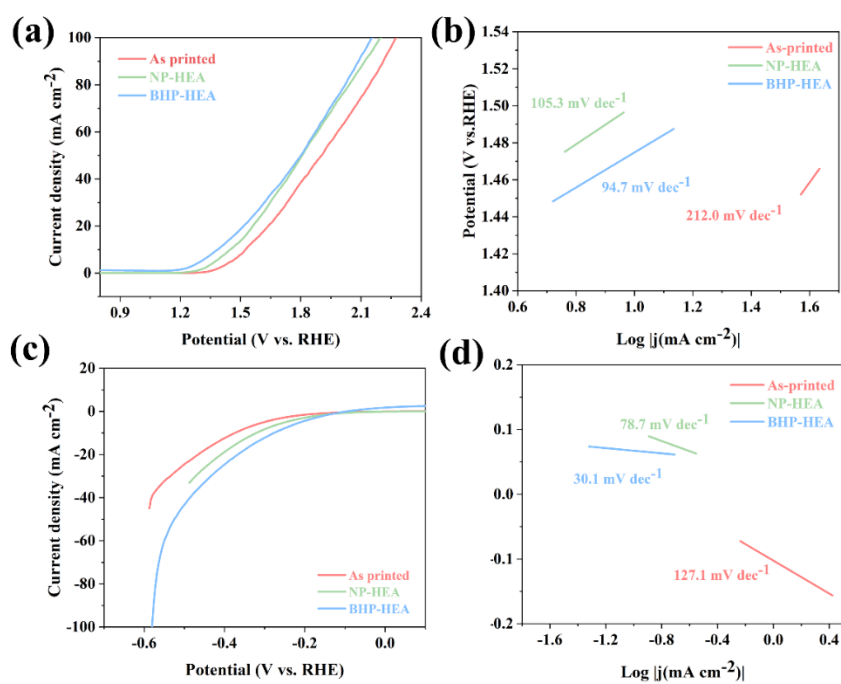
Fig. S5 (a, b) LSV curves and corresponding Tafel plots for OER in 1 M KOH. (c, d) LSV curves and corresponding Tafel plots for HER in 1 M KOH.
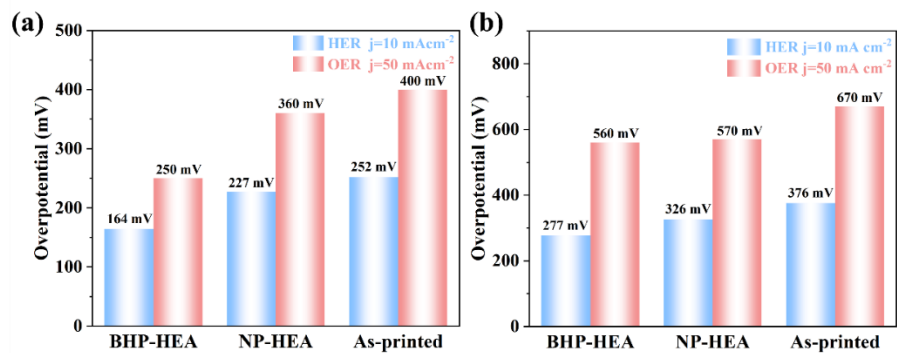
Fig. S6 Overpotential of electrodes in seawater and KOH at the same current density.
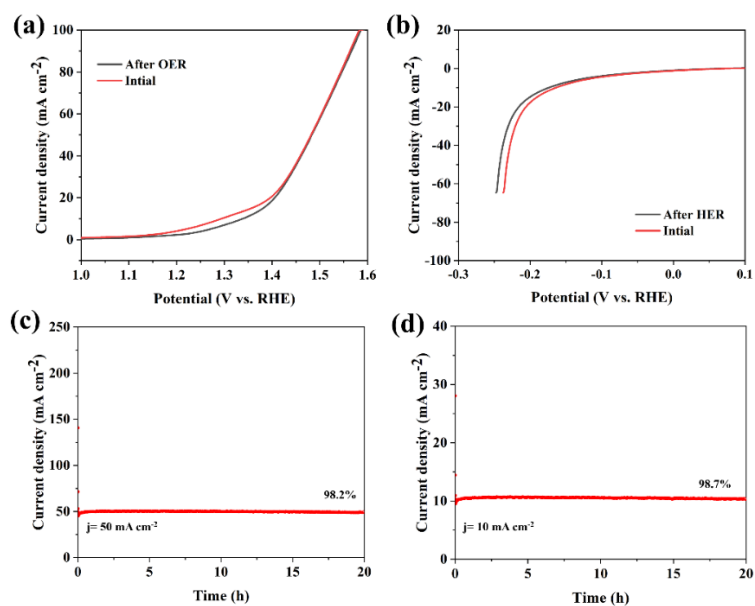
Fig. S7 (a) LSV curves for OER before and after 2000 cyclic voltammograms. (b) LSV curves for HER before and after 2000 cyclic voltammograms. (c) The CA curves recorded at 50 mA cm^{-2} of BHP-HEA electrode for 20 h. (d) The CA curves recorded at 10 mA cm^{-2} of BHP-HEA electrode for 20 h.
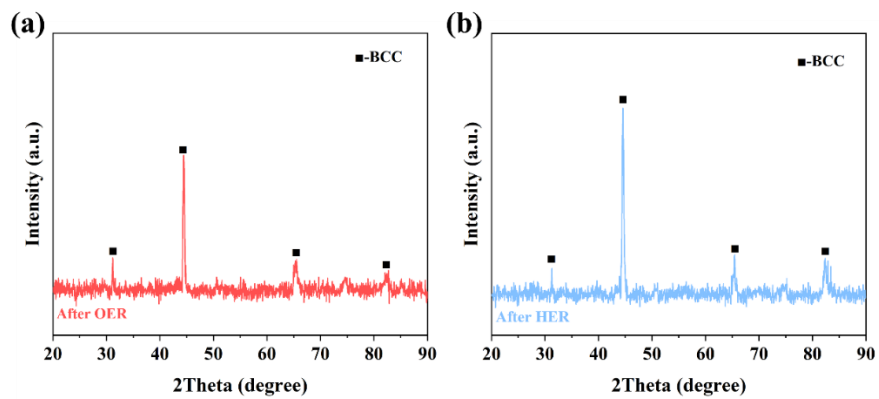
Fig. S8 (a) XRD characterization for electrode after 20 h for OER test in seawater. (b) XRD characterization for electrode after 20 h for HER test in seawater.

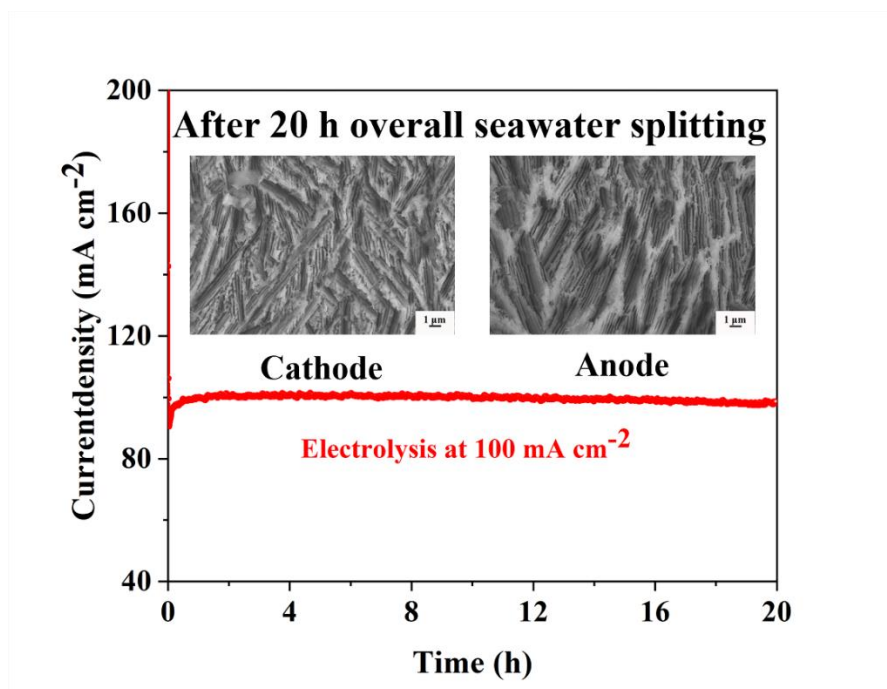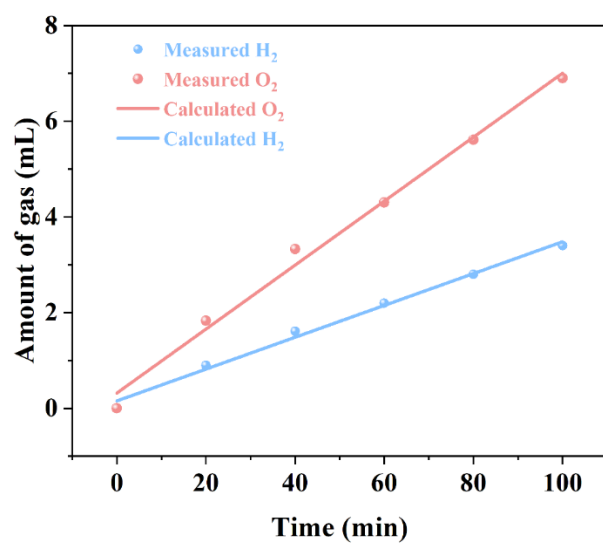**Fig. S9** The stability test results of overall seawater splitting.

Fig. S10 Faradaic efficiency of the BHP-HEA electrolyze.

Table S1. ECSA and TOF of as-printed , NP-HEA, and BHP-HEA electrode.

Catalysts	ECSA (cm^2)	TOF$_{OER}$ (s^{-1})	TOF$_{HER}$ (s^{-1})
As-printed	160.5	0.08	0.02
NP-HEA	407.5	0.317	0.158
BHP-HEA	487.5	0.375	0.187

Table S2. Different metal contents in the HEA electrode before and after stability tests.

Element/at.%	Al	Co	Cr	Fe	Ni
As-printed	16.23	17.64	16.40	17.26	32.47
After SPD	12.64	17.85	17.29	18.59	33.63
After OER	12.45	17.40	18.63	17.80	33.36
After HER	12.27	17.43	19.03	17.83	33.44

Table S3. The cell voltages to achieve 100 mA cm^{-2} for the GHP-HEA electrode, compared with those previously reported catalysts.

Catalysts	Electrolyte	Voltage (V @ mA cm^{-2})	Ref
BHP HEA	Seawater	1.53@100	This work
NiTe@FeOOH	Seawater	1.79@100	[3]
NiFeP-NW-OER	simulated seawater	1.57@100	[4]
C@CoP-FeP/FF	simulated alkaline seawater	1.73@100	[5]
NiMoO$_4$@NiFeP	1 M KOH + seawater	1.71@100	[6]
MoN-Co$_2$N/NF	1 M KOH + seawater	1.70@100	[7]
Pd$_{0.2}$Ni$_{58}$Fe$_{30}$O$_{11.8}$	alkaline seawater	1.76@100	[8]
Mo-CoP$_x$/NF	1 M KO+0.5 M NaCl	2.01@100	[9]
(NiFeCoV)S$_2$/NF	1 M KOH + seawater	1.77@100	[10]
S-NiMoO$_4$@NiFe-LDH	1 M KOH + seawater	1.73@100	[11]
Co-Fe$_2$P	simulated alkaline seawater	1.84@100	[12]
NiFe-PBA-gel-cal	alkaline freshwater	1.66@100	[13]
Ru SAs-MoO$_{3-x}$/NF	alkaline seawater	1.76@100	[14]
NiS@FeNiP/NF	1 M KOH + seawater	1.64@100	[15]
RuO$_2$-Ti$_3$C$_2$/NF	1 M KOH + seawater	1.84@100	[16]

Reference

[1] X. Gu, Ji Y., Tian J., Wu X., Feng L., *Chem. Eng. J.*, 2022, **427**, 131576.

[2] R.Z. He, C.Y. Wang, L.G. Feng, *Chin. Chem. Lett.*, 2023, **34**, 107241.

[3] X.H. Gao, J.L. Chen, Y.H. Yu, F.Y. Wang, X. Wu, X.B. Wang, W.H. Mao, J. Li, W. Huang, Q. Chen, R.S. Li, C.H. You, S.L. Wang, X.L. Tian, Z.Y. Kang, *Chem. Eng. J.*, 2023, **474**, 145568.

[4] J.Y. Li, X. Li, H. Shi, J.H. Luo, L. Wang, J.S. Liang, S.Z. Li, L.M. Yang, T.Y. Wang, Y.H. Huang, Q. Li, *Appl. Catal. B Environ. Energy.*, 2022, **302**, 120862.

[5] J.W. Li, Y.Z. Hu, X. Huang, Y. Zhu, D.L. Wang, *Small.*, 2023 **19**, 2206533.

[6] D.X. Guo, Z. Zhao, M.Y. Zong, C.Z. Fan, W.J. Zheng, D.H. Wang, *ACS Sustain. Chem. Eng.*, 2023, **11**, 8362-8373.

[7] X. Wang, X. Han, R.F. Du, C.C. Xing, X.Q. Qi, Z.F. Liang, P. Guardia, J. Arbiol, A. Cabot, J.S. Li, *ACS Appl. Mater. Interfaces*, 2022, **14**, 41924-41933.

[8] G.R. Xu, N. Zhang, Q.Y. Sun, W. Zhang, Z.X. Wu, L. Wang, *Chem. Eng. J.*, 2023, **476**, 146778.

[9] Y. Yu, J. Li, J. Luo, Z. Kang, C. Jia, Z. Liu, W. Huang, Q. Chen, P. Deng, Y. Shen, X. Tian, *Mater. Today Nano*, 2022, **18**, 100216.

[10] C.R. Feng, M. Chen, Y.F. Zhou, Z.K. Xie, X.M. Li, P. Xiaokaiti, Y. Kansha, A. Abudula, G.Q. Guan, *J. Colloid Interface Sci.*, 2023, **645**, 724-734.

[11] H.Y. Wang, L.Y. Chen, L. Tan, X. Liu, Y.H. Wen, W.G. Hou, T.R. Zhan, *J. Colloid Interface Sci.*, 2022, **613**, 349-358.

[12] S.H. Wang, P. Yang, X.F. Sun, H.L. Xing, J. Hu, P. Chen, Z.T. Cui, W.K. Zhu, Z.J. Ma, *Appl. Catal. B Environ. Energy*, 2021, **297**, 120386.

[13] H. Zhang, S.Y. Geng, M.Z. Ouyang, H. Yadegari, F. Xie, D.J. Riley, *Adv. Sci.*, 2022, **9**, 2200146.

[14] D. Feng, P.Y. Wang, R. Qin, W.J. Shi, L. Gong, J.W. Zhu, Q.L. Ma, L. Chen, J. Yu, S.L. Liu, S.C. Mu, *Adv. Sci.,* 2023, **10**, 2300342.

[15] J.T. Ren, L. Chen, W.W. Tian, X.L. Song, Q.H. Kong, H.Y. Wang, Z.Y. Yuan, *Small*, 2023, **19**, 2300194.

[16] Y. Zhang, Z.H. Zhang, Z.R. Yu, A. Addad, Q. Wang, P. Roussel, S. Szunerits, R. Boukherroub, ACS *Appl. Mater. Interfaces*, 2023, **15**, 58345-58355.